Supplementary Information

Changes in neural network homeostasis trigger neuropsychiatric symptoms

Aline Winkelmann[1,2], Nicola Maggio[3], Joanna Eller[4], Gürsel Caliskan[5], Marcus Semtner[2], Ute Häussler[6], René Jüttner[7], Tamar Dugladze[4], Birthe Smolinsky[8], Sarah Kowalczyk[8], Ewa Chronowska[9], Günter Schwarz[8], Fritz G. Rathjen[7], Gideon Rechavi[10], Carola A. Haas[6,11], Akos Kulik[9,12], Tengis Gloveli[4,13], Uwe Heinemann[5] and Jochen C. Meier[2]

1 FU-Berlin, Fachbereich Biologie, Chemie, Pharmazie, Takustr. 3, 14195 Berlin
2 RNA editing and Hyperexcitability Disorders Helmholtz Group, Max Delbrück Center for Molecular Medicine, 13092 Berlin, Germany
3 Talpiot Medical Leadership Program, Department of Neurology and the J. Sagol Neuroscience Center, The Chaim Sheba Medical Center, 52621 Tel HaShomer, Israel
4 Cellular and Network Physiology Group, Institute of Neurophysiology, Charité Universitätsmedizin Berlin, 10117 Berlin, Germany
5 CC2 Zentrum für Physiologie, Freie Universität Berlin, 14195 Berlin, Germany
6 Experimental Epilepsy Research, Dept. of Neurosurgery, Neurocenter, University of Freiburg, 79106 Freiburg Germany
7 Developmental Neurobiology, Max Delbrück Center for Molecular Medicine, 13092 Berlin, Germany
8 Institute of Biochemistry, University of Cologne & Center for Molecular Medicine 50674 Cologne, Germany
9 Department of Physiology II, University of Freiburg, D-79104 Freiburg, Germany
10 Sheba Cancer Research Center, The Chaim Sheba Medical Center and Sackler Faculty of Medicine, Tel Aviv University, 69978 Tel Aviv, Israel
11 BrainLinks-BrainTools, Cluster of Excellence, University of Freiburg, Germany
12 BIOSS Centre for Biological Signalling Studies, University of Freiburg, D-79104 Freiburg, Germany
13 Bernstein Center for Computational Neuroscience Berlin, Unter den Linden 6, 10099 Berlin, Germany

Correspondence:
Dr. Jochen C. Meier
Max Delbrück Center for Molecular Medicine
Robert-Rössle-Str. 10, 13092 Berlin
Germany
Phone: +49-(0)30-9406-3062
Fax: +49-(0)30-9406-3819
Email: jochen.meier@mdc-berlin.de

Short title: Neuron type-specific impact on behavior

Supplementary Methods

Molecular cloning and constructs

Total RNA was isolated from adult rat cortex using TRIzol® Reagent (Invitrogen Life Technologies), and cDNA was synthesized from 2 µg RNA using SuperScript II reverse transcriptase (Invitrogen). Poly-A tail anchored oligonucleotides (equimolar mixture of 3'-anchored poly-T oligonucleotides $T_{18}V$, $T_{15}V$, $T_{13}V$) were used for transcription of mRNA into cDNA. For cloning of the large cytoplasmic loops between transmembrane domains 3 and 4 (TM3-4) of GlyR α3 splice variants L and K (1) the loop sequences were amplified with PCR using oligonucleotides 5'-ACCATGTCAAGGCAACACAAA GAACTG -3' and 5'-TTTACCGGTCGGGAAATGGTGTCAATCTTC-3' and ligated with an in-house made TA cloning vector (derived from pBluescript). Next, the TM3-4 loops were cloned in frame with the DsRed-Express coding sequence of pDsRed-Express-N1 (Clontech Laboratories, Inc) using *Xho*I and *Age*I restriction enzymes. Note that the GlyR α3 TM3-4 loop harbors a nucleus localization sequence ['NLS', see Suppl. Fig. 2 for details, (2)].

SEC8-coding cDNA was amplified by PCR with oligonucleotides 5'-ATGGCGGCAGAAGCAGCTGG-3' and 5'-TCACACAGTGGTTATTTTCTTGTCCTTGG-3', and PCR products were ligated with our in-house TA vector derived from pBluescript. Different regions covering the GlyR α3-intrinsic NLS (RRKRK and RFRRKRKNK), and a conventional NLS sequence (KKKRK) were attached to the N-terminus of SEC8 using site-directed mutagenesis (GeneEditor, Promega, Madison, WI, USA) with following 5'-phosphorylated oligonucleotides: 5'-GCAGGAATTCGATATGAAGAAGAAGAGGAAAGCGGCAGAAGCAG-3', 5'-CTGCAGGAATTCGATATGAGGAGGAAGAGGAAAGCGGCAGAAGCAG-3', or 5'-CTGCAGGAATTCGATATGAGGTTTAGGAGGAAGAGGAAAAACAAGGCGGCAGAAGCAG-3'. Next, the NLS-harboring SEC8 clones were amplified with PCR using oligonucleotides 5'-GGCAAGCTTATGAAGAAGAAGAGGAAAGCGGCAG-3', 5'-GGCAAGCTTATGAGGTTTAGGAGGAAGAGGAAAA-3' or 5'-GGCAAGCTTATGAGGAGGAAGAGGAAAGCGGC-3' and 5'-GGCGGATCCAATCCCACAGTGGTTATTTTCTTGTCC-3', and cloned in frame with the EGFP-coding sequence of pEGFP-N1 (Clontech) using *Hind*III and *BamH*I restriction enzyme sites.

For co-sedimentation experiments GlyR α3K and α3L large cytoplasmic loops were amplified with PCR and transferred into pGEX-6P-1 (New England Biolabs, Ipswich, MA, USA) using *BamH*I and *Eco*RI restriction enzymes.

Human synapsin 1 (Syn1) promotor was provided by Susanne Schoch (University of Bonn, Institute of Neuropathology, Bonn, Germany), Cre-recombinase was provided by Sebastian Auer (Max Delbrück Center for Molecular Medicine, Berlin, Germany), and AmCyan was cloned from pAmCyan (Clontech, PT3477-5). The 2A self-processing peptide EGRGSLLTCGDVEENPGP (3) was used for bicistronic expression of AmCyan and Cre-recombinase. Syn1-AmCyan and Syn1-AmCyan-2A-Cre constructs were generated using standard molecular techniques.

Quantification of the fraction of GlyR $\alpha3^{185L}$-coding mRNA

The fraction of $\alpha3L^{185L}$-coding mRNA was quantified by applying our quantitative cloning approach described earlier (4, 5). However, as GlyR knockin mice express a $\alpha3L^{185L}$-coding cDNA copy, contamination of RNA with genomic DNA needed to be minimized. To this end, 50 µg RNA were incubated for 15 minutes at 37°C with RNase-free DNase (Roche Applied Science, Mannheim, Germany) and purified using RNeasy Spin Columns (Stratec Molecular GmbH, Berlin, Germany). To verify degradation of genomic DNA in RNA preparations, PCR was performed on samples that were processed in the absence of reverse transcriptase.

Single cell PCR

Cytosols of neurons were gathered with the recording pipette. The pipette tip was broken into a PCR tube and immediately shock-frozen in liquid nitrogen. Fast-spiking interneurons were identified on the basis of anatomical position and shape of somata, and electrophysiological characteristics (action potential duration and firing pattern, shape of after-hyperpolarization). Reverse transcription was performed in recording pipette tip-containing PCR tubes in a total volume of 5 µl using RNase-free materials and solutions under sterile conditions. Then, 1.5 µl of the synthesized cDNA was used for amplification of *Glra2*-, *Glra3*- and *Gapdh*-coding gene transcripts. Three consecutive nested PCRs were performed using oligonucleotides and PCR programs listed in Suppl. Table 3 and 4, respectively.

Western blot

Proteins were separated by running the gel for 1 h at 35 mA (Mini-PROTEAN Tetra System, Bio-Rad Laboratories, Hercules, CA, USA). Next, proteins were blotted on a nitrocellulose membrane (0.45 µm, Bio-Rad Laboratories) by applying 2 mA/cm^2. After blotting, the membrane was washed once with TBST-buffer (100 mM Tris/HCl pH 7.4, 154 mM NaCl, and 0.1% Tween20) and then blocked with 5% goat or donkey serum in TBST for at least 1 h at room temperature. Three TBST wash steps were performed before the membrane was incubated over night at 4°C with a rat monoclonal anti-HA antibody (3F10, 0.1 µg/ml, Roche Applied Science, Mannheim, Germany) or a rabbit polyclonal anti-tubulin antibody (1:1000, Cell Signaling). Secondary HRP-conjugated goat anti-rat and donkey anti-rabbit antibodies (both 1:10,000, Jackson ImmunoResearch Laboratories, West Grove, PA, USA) were applied after four wash steps in TBST and incubated for 90 min at room temperature. After three final wash steps in TBST, signal detection was performed using Immun-Star™ WesternC™ Chemiluminescence in combination with Molecular Imager ChemiDoc XRS System (Bio-Rad Laboratories).

Analyses of behavior

Behavioral tests were performed in temperature-controlled (24-26°C) rooms. **Accelerating Rotarod:** Mice were placed onto the rod (diameter 3.6 cm) apparatus to assess differences in motor coordination and balance. The animals were habituated by receiving training sessions of two trials, sufficient to reach a baseline level of performance. Then each mouse underwent three trials (with a 10 minutes interlude) with increasing speed. The initial speed was set a 1.0 rpm and raised every 30 s. Latency to fall was calculated as an average of the mean time (s) each mouse fall off the rod over

the three consecutive trials (6). **Sucrose Preference Test:** Prior to performance of the test, mice were habituated to the presence of two drinking bottles in their home cage. During the execution of the test, mice were given, for 24 h, a free choice between two bottles, one with 1% sucrose solution and another with tap water. To prevent possible effects of side preference in drinking behavior, the position of the bottles was switched after 12 h. No previous food or water deprivation was applied before the test. The consumption of water and sucrose solution was estimated simultaneously by weighing the bottles. The sucrose intake was calculated as an amount of consumed sucrose in mg per gram body weight. The preference for sucrose was calculated as a percentage of consumed sucrose solution of the total amount of liquid drunk (7). **Light-dark preference test:** The dark/light box consisted of two plexiglass compartments, one black/dark (15 ×20 ×25 cm^3) and one lit (30 ×20 ×25 cm^3), connected by a hole. Mice were placed into the dark compartment, from where they could visit the lit box, illuminated by light of 50 lx intensity. Latency to exit from the dark box (s) as well as the time spent in the light box (%) were measured. Total length of the trial was 5 minutes (7). **Elevated Plus Maze:** Mice were placed at the junction of the four arms of the maze, facing an open arm. Entries as well as time spent in open arms (%) were measured for 5 min. An increase in open arm activity (duration and/or entries) reflects anti-anxiety behavior (8). **Open Field:** Mice were allowed to freely behave in a squared arena (40.6 cm*40.6 cm) for 5 minutes. The behavior was scores as it follows: lines crossed: total amounts of lines drawn at the floor crossed during the trial, entries to the center: number of the time the animals entered in to the center of the arena, rearings: number of time the mice stood on their hind legs in the maze, freezing: time (s) in which the mice were completely stationary (9). **Novel Object Recognition:** The object recognition task evaluates recognition memory, and it is based on the propensity of rodents to discriminate a familiar object from a new one. Mice were individually habituated to an open field box for 5 min, the day before the test. During the acquisition phases, two objects of identical material were placed in a symmetric position within the chamber for 5 min duration. At 24 h after acquisition phase training, one of the objects was replaced by a novel one, and exploratory behavior was again evaluated for 5 min. Exploration of an object was characterized as rearing on it or sniffing it at a distance of less than 2 cm and/or touching it with the nose. Successful recognition was revealed by preferential exploration of the novel object. Discrimination of novelty was assessed by a preference index (10), determined as: (time near the new - time near the old object)/(time near the new + time near the old object). **Radial Maze:** The test was conducted as previously described (11). Briefly, the apparatus consisted of eight arms (32 cm*8 cm*19 cm) extending radially from an octagonal central area (20 cm across). Beginning on the day prior to the adaptation phase, the animals were food deprived while being allowed access to water. During the adaptation phase, food was inserted in the wells of 4 chosen arms. Each mouse was placed in the central area of the radial maze with all arm entries closed. After 10 s, the doors of the 4 baited arms were opened and the animals were allowed to explore them for 10 minutes while the remaining arms were kept close. Following the adaptation phase, mice were trained for 9 consecutive days with one trial/day. Each mouse was placed in the center of the maze with all arm entries closed. After 10 s, the doors were opened and the mouse was permitted to enter any of the eight arms. Only 4 of the eight arms contained the food pellet. An arm entry was scored

when the mouse had all four paws within an arm. A trial was terminated after either all the bait was consumed or after 10 minutes had elapsed, whatever occurred first. Two scores were calculated: 1) reference memory errors: entries into an arm which was never baited and 2) working memory errors: re-entries into an arm visited on the ongoing trial.

Supplementary Tables

Suppl. Table 1: New GlyR α3L interaction partners identified using GST pulldown and mass spectrometry, listed in the alphabetical order of gene names. Mowse scores above 53 indicate significant ($P < 0.05$) hits.

Protein	Gene	Matched peptides	Mowse score
5'-AMP-activated protein kinase subunit γ2	*Aakg2*	15	54
β-Actin	*Actb*	17	85
γ-Actin	*Actg*	18	93
AP-2 adaptor complex subunit α1	*Ap2a1*	29	112
AP-2 adaptor complex subunit α2	*Ap2a2*	26	92
AP-2 adaptor complex subunit β1	*Ap2b1*	21	61
Caspase-1 precursor	*Casp1*	17	58
Chondroitin sulfate synthase-1	*Chss1*	21	54
ATP-dependent RNA helicase (Dead box protein 1)	*Ddx1*	21	60
Dihydropyrimidinase-related protein 2	*Dpyl2*	21	92
Early endosome antigen-1	*Eea1*	34	61
Exocyst complex	*Exoc4*	18	57
HECT domain and RCC1-like domain-containing protein 2	*Herc2*	33	56
Heterogeneous nuclear ribonucleoprotein K	*Hnrpk*	19	62
Heat shock 70 kDa protein 8	*Hsp7c*	13	63
Karyopherin (Importin) β1	*Ipo8*	12	77
Cytokeratin-14	*K1c14*	19	63
Cytokeratin-17	*K1c17*	20	93
Cell surface glycoprotein MUC18 precursor	*Muc18*	16	58
Nucleoside diphosphate kinase 7 (nm23-M7)	*Ndk7*	14	60
Phosphatidylinositol-4-phosphate 5-kinase type-1 γ	*Pi51c*	16	58
Transcriptional activator protein Pur-alpha	*Pura*	18	74
PC4 and SFRS1-interacting protein	*Psip1*	9	54

Suppl. Table 2: Overview of oligonucleotides and PCR programs for genotyping.

Camk2a^{Cre}	5'-GGTTCTCCGTTTGCACTCAGGA-3' 5'-CCTGTTGTTCAGCTTGCACCAG-3' 5'-CTGCATGCACGGGACAGCTCT-3'
Pvalb^{Cre}	5'-GCGGTCTGGCAGTAAAAACTATC-3' 5'-GTGAAACAGCATTGCTGTCACTT-3'
Hprt$^{\alpha 3L185L}$	5'-ACGTCAGTAGTCATAGGAACTGCGGTCG-3' 5'-ACACCATCTCCCGAGCCTGCTTTC-3', and 5'-TGTCCTTAGAAAACACATATCCAGGGTTTAGG-3' 5'-CTGGCTTAAAGACAACATCTGGGAGAAAAA-3'
PCR program	2' 94°C – [30'' 94°C – 30'' 65°C – 1' 68°C] – 8' 72°C - ∞ 4°C ----------38 cycles----------

Suppl. Table 3: Oligonucleotides used for single cell nested PCRs

	Target gene transcripts	Oligonucleotides
1st PCR	*Glra2*	5'-GGATATGATGCAAGAATCAGGC-3' 5'-CATCTGGATCAAATAGTAGCCC-3'
	Glra3	5'-GATCTCAAGAATTTCCCAATGG-3' 5'-GCTGAGAACACAAAAAGGAGG-3'
	Gapdh	5'-CCACTCACGGCAAATTCAACG-3' 5'-AGCCCAAGATGCCCTTCAGTG-3'
2nd PCR	*Glra2*	5'-ACCGAGTGAATATTTTTCTGAGAC-3' 5'-GTGAAACTTGACCTCAATGCAG-3'
	Glra3	5'-TGGGTACACAATGAATGATCTC-3' 5'-GCCATCCAAATGTCAATAGCC-3'
	Gapdh	5'-ACCATCTTCCAGGAGCGAGAC-3' 5'-CTCAGATGCCTGCTTCACCAC-3'
3rd PCR	*Glra2*	5'-GAATGATTCACGGCTGGCATACAG-3' 5'-GCTCCTTCTCTTCTTTCAAAATAATCCGG-3'
	Glra3	5'-GGCTGAAGGACTCACTAAGC-3' 5'-TTGACATAGGACACCTTTGG-3'
	Gapdh	5'-GGTGCTGAGTATGTCGTGGAG-3' 5'-ATGCAGGGATGATGTTCTGG-3'

Suppl. Table 4: PCR programs used for single cell nested PCRs

1st-3rd PCR	*Gapdh*	2' 94°C – [1' 94°C – 1' 56°C – 1'30'' 72°C] – 10' 72°C – ∞ 4°C ----------35 cycles----------
1st and 2nd PCR	*Glra2*/*Glra3*	2' 94°C – [45'' 94°C – 1' 56°C – 1' 72°C] – 10' 72°C – ∞ 4°C ----------45 cycles----------
3rd PCR	*Glra2*/*Glra3*	2' 94°C – [45''94°C – 1' 50°C – 1' 72°C] – 10' 72°C – ∞ 4°C ----------45 cycles----------

Supplementary Figures

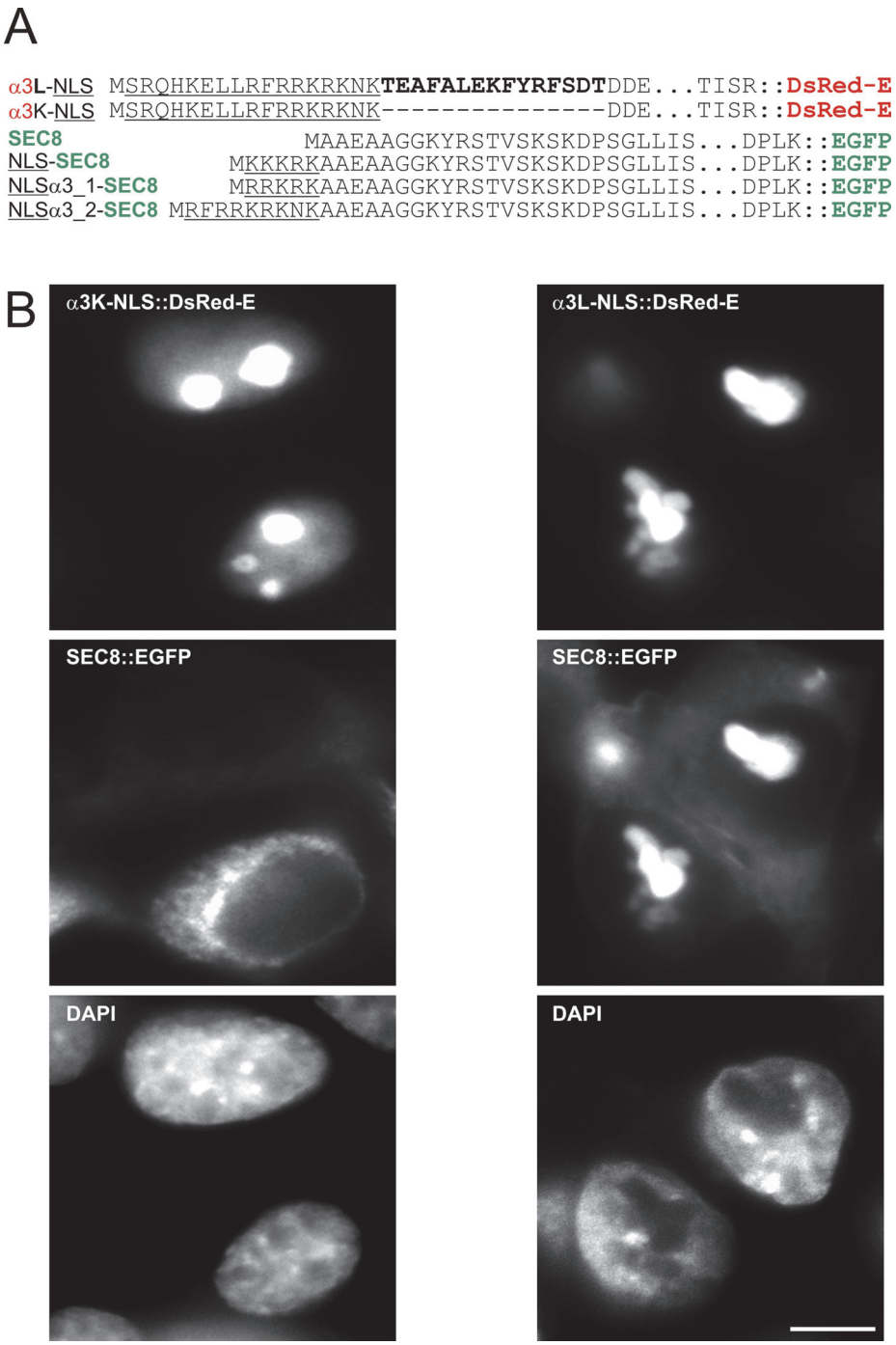

Suppl. Figure 1: The large cytoplasmic loop of GlyR α3L translocates SEC8::EGFP to the nucleus of HEK293 cells. (A) Sequence information about the molecular constructs. The large cytoplasmic loops between transmembrane domains 3 and 4 (TM3-4) of GlyR α3K and α3L were fused to DsRed-Express (DsRed-E), and SEC8 with or without nucleus localization signals (NLS) was tagged with EGFP. Note the GlyR α3-intrinsic NLS (RRKRK) in the N-terminal region (underlined) of the loop. (B) Grey scale images of transfected cells shown in Figure 1C. See Supplementary Figure 2 and Table 1 for information about quantitative data. Scale bar: 10 µm.

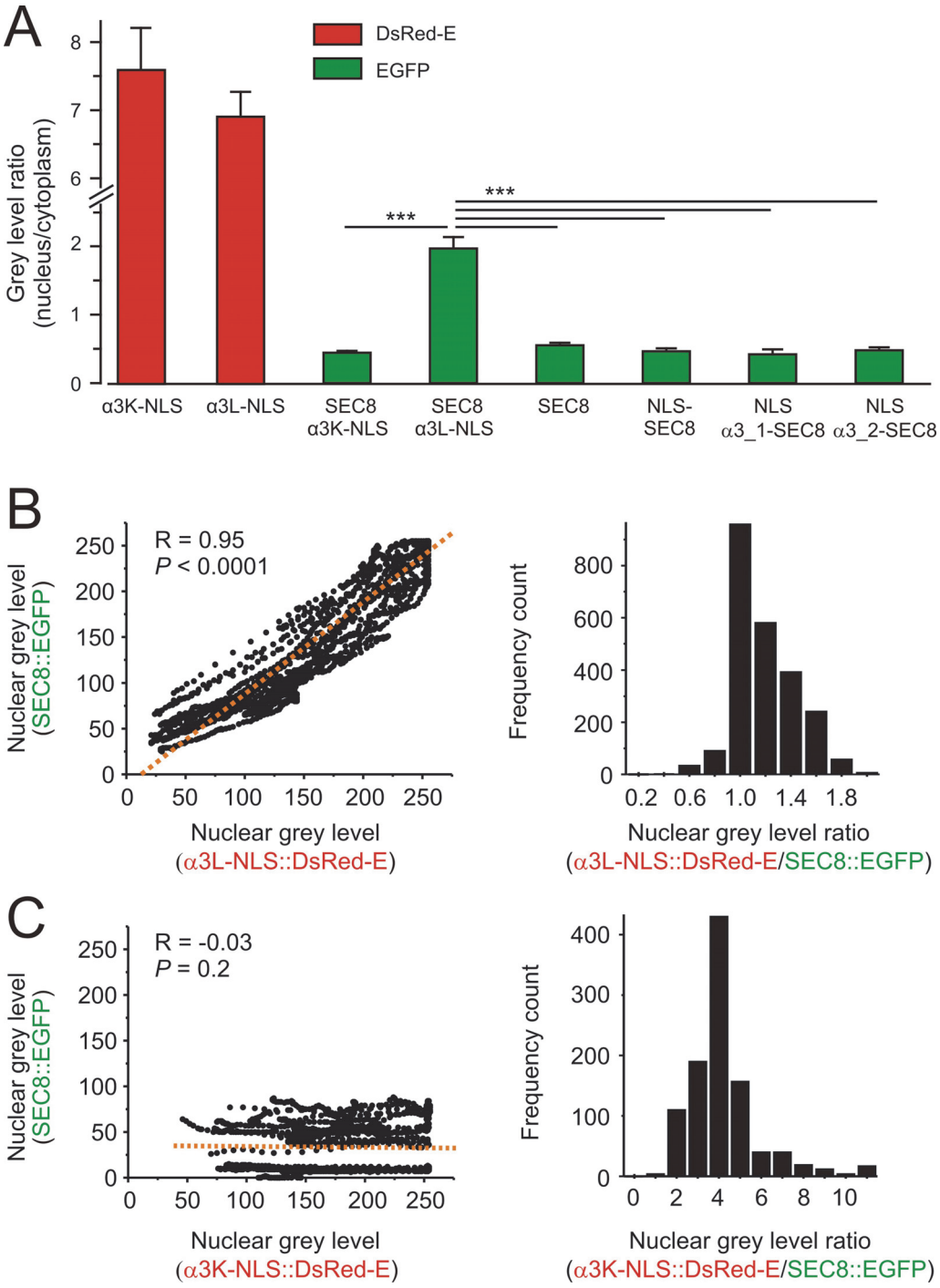

Suppl. Figure 2: Quantification of integrated fluorescence intensities in transfected HEK293 cells. (A) Summary of the calculation of ratios between integrated fluorescence intensities measured within circular regions of interest (5 µm diameter) centered on nucleus and positioned on perinuclear regions of the soma revealed nuclear targeting of both α3K-NLS::DsRed-E and α3L-NLS::DsRed-E loops (red bars). However, only the α3L-NLS::DsRed-E loop significantly increased the ratio of integrated SEC8::EGFP fluorescence intensities measured between nucleus and cytoplasm, indicating that SEC8::EGFP was translocated to the nucleus of

α3L-NLS::DsRed-E-expressing HEK293 cells. Different SEC8::EGFP variants expressed alone were not able to (B, C) Quantitative analysis using line scans (10 µm length) in the nucleus revealed excellent positive correlation (R = 0.95) of locally corresponding α3L-NLS::DsRed-E and SEC8::EGFP, not α3K-NLS::DsRed-E and SEC8::EGFP, signal intensities. Histograms right-hand show distributions of nuclear grey level ratios calculated between pixel intensities of locally corresponding α3 loop and SEC8 signals. A value of 1 represents perfect signal overlap. Representative images showing subcellular distribution patterns of the different constructs are shown in Supplementary Figure 3. Data represent means ± standard error. Statistical significance is indicated as ***: $P < 0.001$.

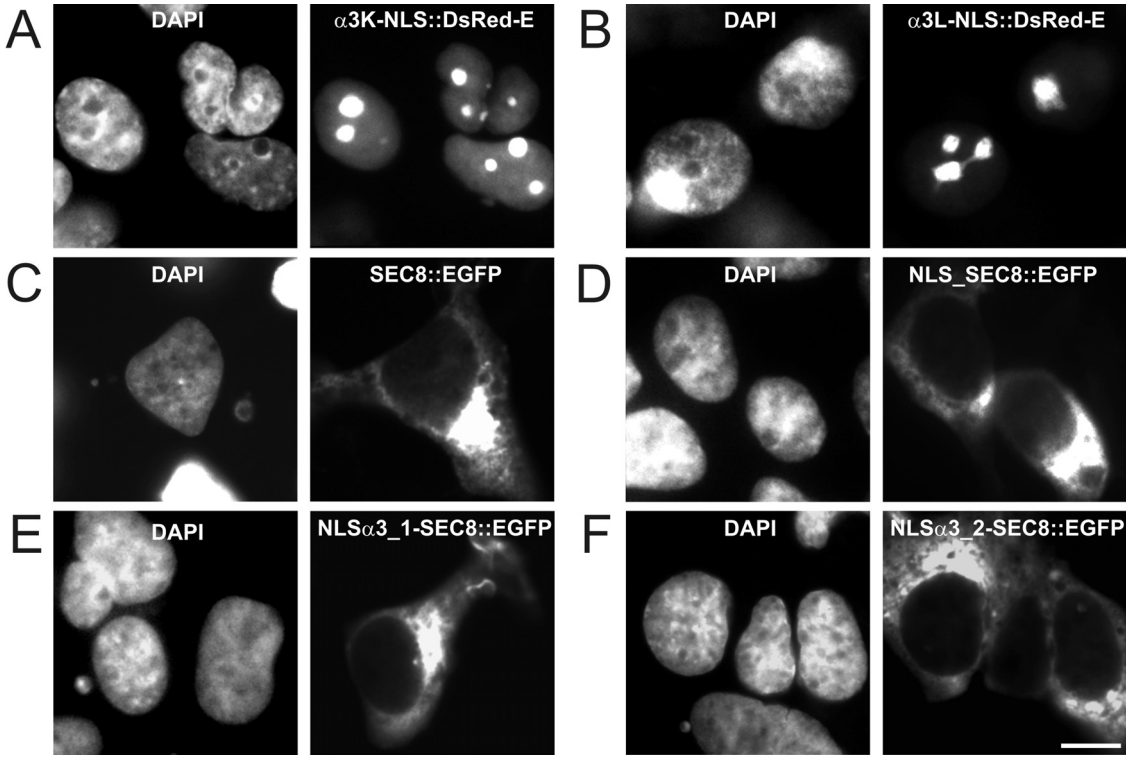

Suppl. Figure 3: Representative images of subcellular expression patterns of GlyR α3K and α3L cytoplasmic loops and SEC8 with or without different NLS in HEK293 cells are shown. (A, B) The GlyR α3-intrinsic NLS in the large cytoplasmic loops between TM3 and 4 of the α3K and α3L RNA splice variants are effective in HEK293 cells. (C-F) Neither SEC8::EGFP nor SEC8::EGFP equipped with different NLS (shown in Suppl. Figure 1A) targeted the nucleus of HEK293 cells. See Supplementary Figure 2 and Table 1 for information about quantitative data. Scale bar: 10 µm.

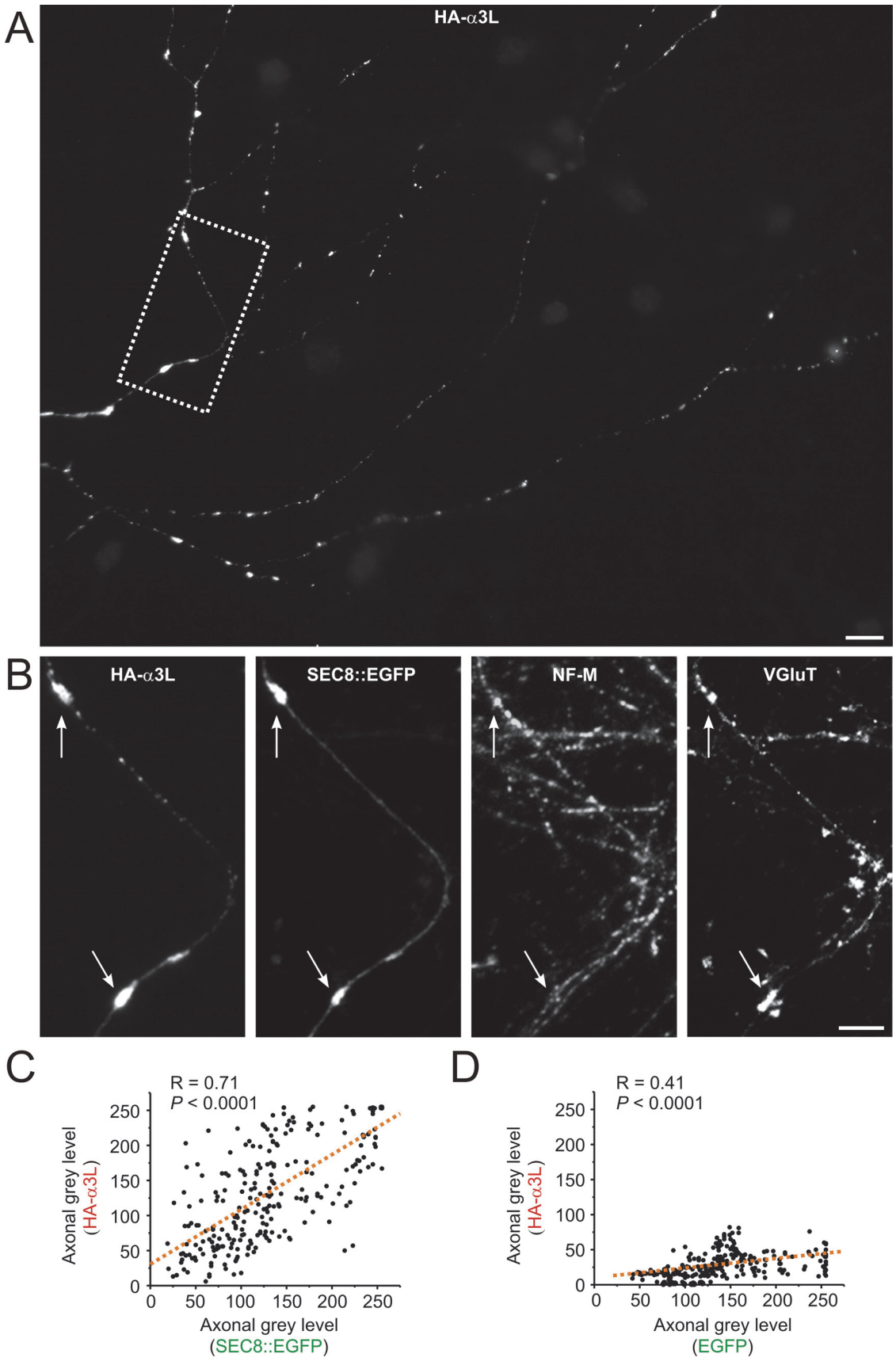
A
HA-α3L
B
HA-α3L
SEC8::EGFP
NF-M
VGluT
C
R = 0.71
P < 0.0001
Axonal grey level
(HA-α3L)
Axonal grey level
(SEC8::EGFP)
D
R = 0.41
P < 0.0001
Axonal grey level
(HA-α3L)
Axonal grey level
(EGFP)

Suppl. Figure 4: SEC8::EGFP facilitates axonal trafficking of full-length GlyR HA-α3L. (A) Image showing the distribution of HA-α3L in the axonal compartment of a co-transfected neuron. (B) High-power views of the boxed region (A) indicate the cozy relationship between HA-α3L, the axonal marker neurofilament-M (NF-M) and the vesicular glutamate transporter VGluT. (C, D) Quantitative analysis using line scans (10 µm length) of the proximal part of the NF-M-positive axons (< 100 µm distance from the soma) revealed strong positive correlation (R = 0.71) of locally corresponding SEC8::EGFP and GlyR HA-α3L signal intensities (C). In contrast, when EGFP was co-expressed with GlyR HA-α3L, correlation was only weakly positive (R = 0.41) (D). See also Table 2 for information about quantitative data on relative axonal versus cytoplasmic versus dendritic GlyR HA-α3L integrated signal intensities. Scale bars: 10 µm (A), and 5 µm (B).

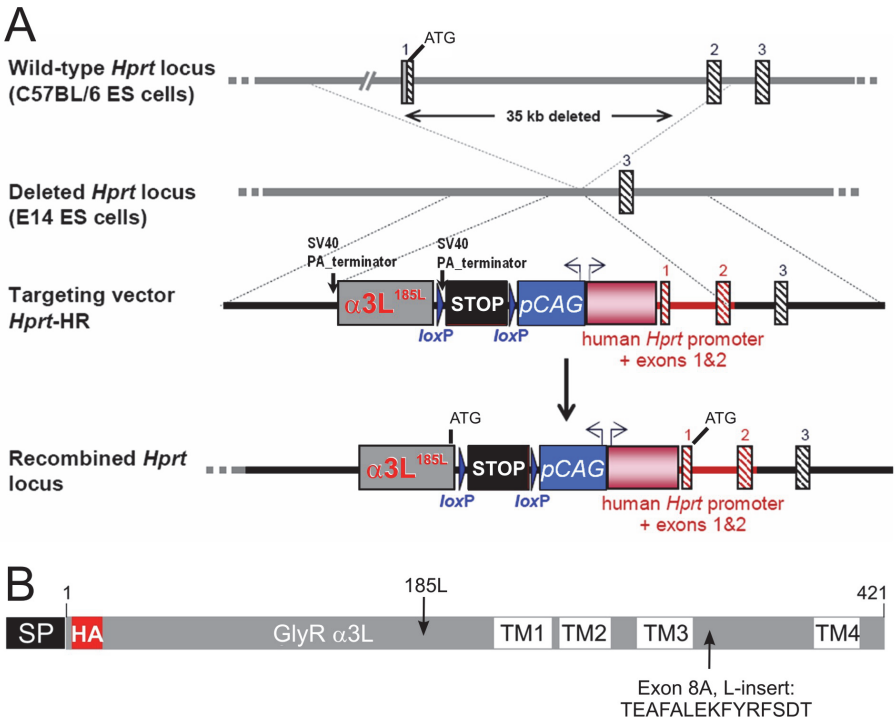

Suppl. Figure 5: Generation of the GlyR HA-α3L^{185L}-knockin mouse line for cell type specific expression. (A) Homologous recombination of genOway's "Quick Knock-in^{TM}" targeting vector with the CAG promoter (pCAG), a floxed STOP cassette (*lox*P sites), and the cDNA coding for HA-tagged GlyR α3L^{185L} (B) repairs the *Hprt* gene locus on the X-chromosome ('*Hprt*-HR'). HA = hemagglutinin epitope tag, SP = signal peptide, SV40-PA = SV40-derived poly-adenylation signal, TM = transmembrane domain.

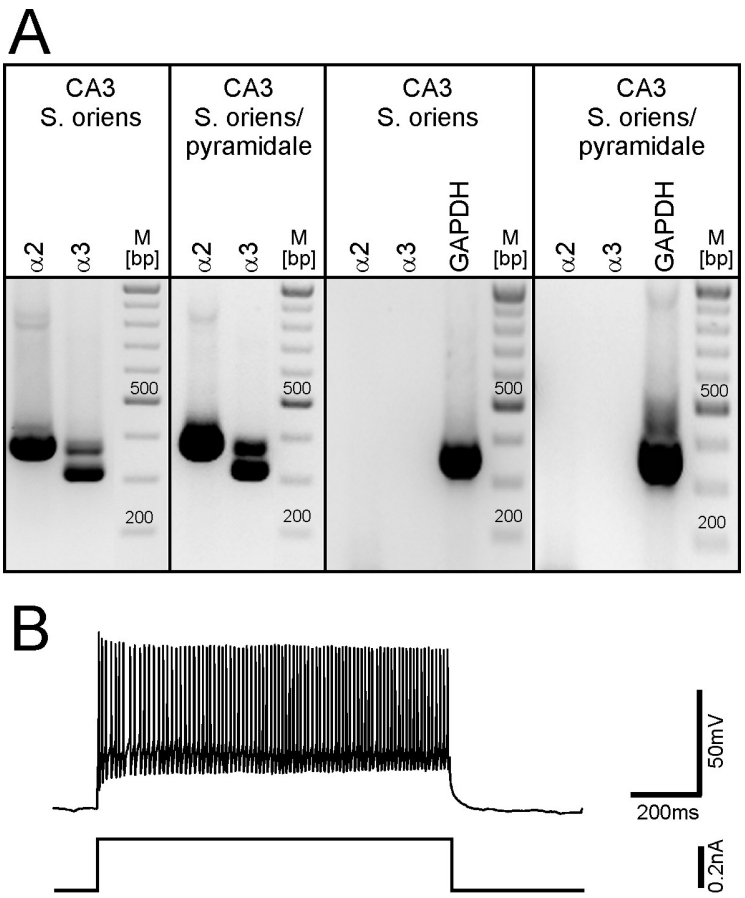

Suppl. Figure 6: Single cell RT-PCR amplification of GlyR α2- and α3-coding mRNAs from fast-spiking interneurons in wildtype mice. (A) Agarose gels show co-expression of GlyR α2 and α3 in 2 out of 4 investigated interneurons. Amplification of mRNA coding for the house keeping gene *Gapdh* verified presence of cDNA in case of GlyR α2- or α3-negative samples. (B) Characteristic fast-spiking pattern of an investigated interneuron in CA3 (*stratum oriens*/*pyramidale*) recorded in the current-clamp mode. To elicit action potential firing, the patched interneuron was depolarized by 0.3 nA current injection, starting from a resting membrane potential of -65 mV (-0.1 nA holding current).

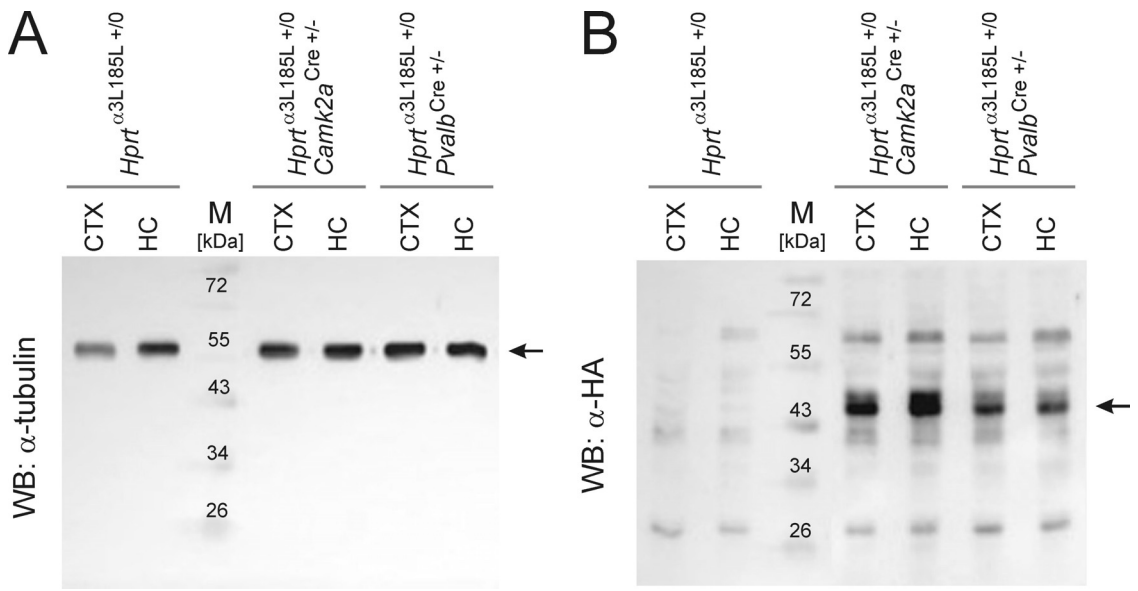

Suppl. Figure 7: Western blot analysis of protein lysates obtained from cortex (CTX) and hippocampus (HC) of control animals (*Hprt*$^{\alpha 3L185L\ +/0}$) and mice with targeted GlyR HA-α3L^{185L} expression in principal glutamatergic neurons (*Hprt*$^{\alpha 3L185L\ +/0}$; *Camk2a*$^{Cre\ +/-}$) or parvalbumin-positive interneurons (*Hprt*$^{\alpha 3L185L\ +/0}$; *Pvalb*$^{Cre\ +/-}$). Protein bands corresponding to the loading control tubulin (A) and full-length (48 kDa) GlyR HA-α3L^{185L} (B, α-HA) are indicated with arrows.

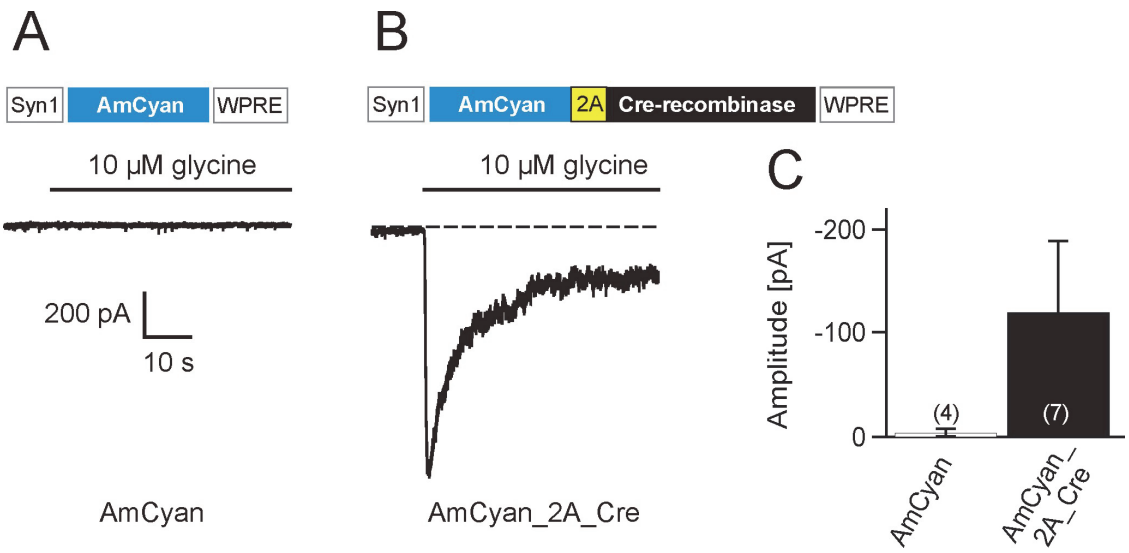

Suppl. Figure 8: Analysis of high affinity type (185L) GlyR α3L in primary hippocampal neuron cultures of GlyR knockin animals. (A) A synapsin-1 promoter-dependent construct was used for expression of AmCyan fluorescent protein, and transfected hippocampal neurons did not show significant transmembrane chloride currents (-50 mV) upon application of a low dose of glycine (10 µM) which does not activate non-RNA-edited hippocampal GlyRs. (B) Same approach except that a construct for bicistronic expression of AmCyan and Cre-recombinase was used. In this case, transfected neurons responded to 10 µM glycine. (C) Quantification of glycine effects on membrane currents. This electrophysiological data confirms Cre-recombinase-dependent targeted GlyR $\alpha 3L^{185L}$ protein expression. Data represent means ± standard error.

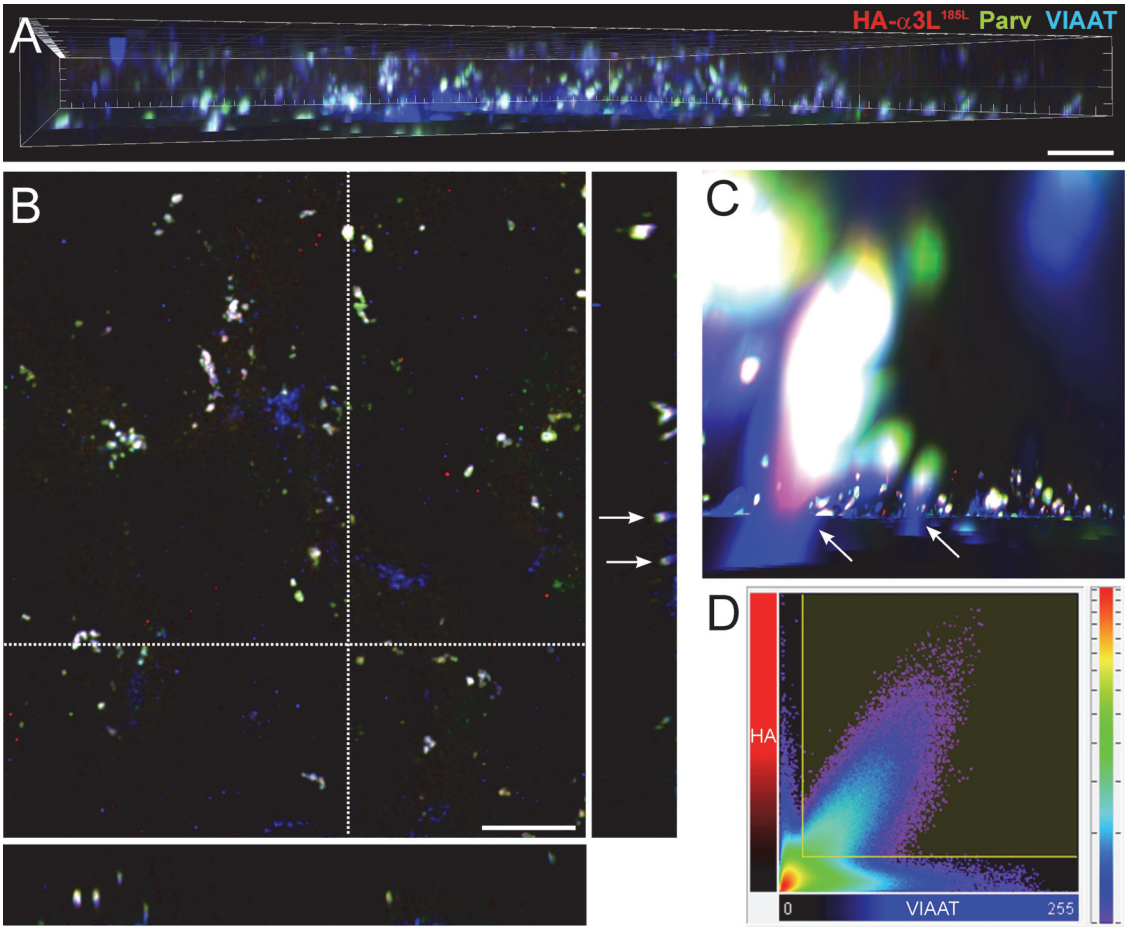

Suppl. Figure 9: Immunochemical evidence for presynaptic GlyR $\alpha 3L^{185L}$ protein expression in *Hprt*$^{\alpha 3L185L\ +/0}$; *Pvalb*$^{Cre\ +/-}$ animals. (A) Side view of a 3D reconstructed area in *stratum pyramidale* composed of 75 serial confocal multi-channel images (thickness of optical slice: 9.45 µm; voxel size: X, Y: 0.115 µm, Z: 0.126 µm). Fluorescent signals correspond to GlyR HA-$\alpha 3L^{185L}$ (red), parvalbumin (Parv, green), and VIAAT (blue). White color indicates co-localization of the three investigated proteins. (B) Representative confocal plane taken from the middle of the Z-stack shown in A. Dotted lines indicate positions of Z-sections along X and Y axes (0.230 µm thick) shown below (X) and right hand (Y) to the image. Arrows mark cross-sectioned presynaptic boutons with neck and head shown at higher magnification in the zoomed 3D view (C). (D) Color-coded example scatter plot showing the frequency distribution of signal intensities corresponding to VIAAT and HA-$\alpha 3L^{185L}$. The yellow rectangle indicates thresholds for each fluorophore, and in this example 183,419 voxels above thresholds were used for calculation of the Pearson's correlation coefficient. The Mander's overlap coefficient provides quantitative information about the degree of threshold-independent congruency of co-localized signals. Scale bars: 10 µm.

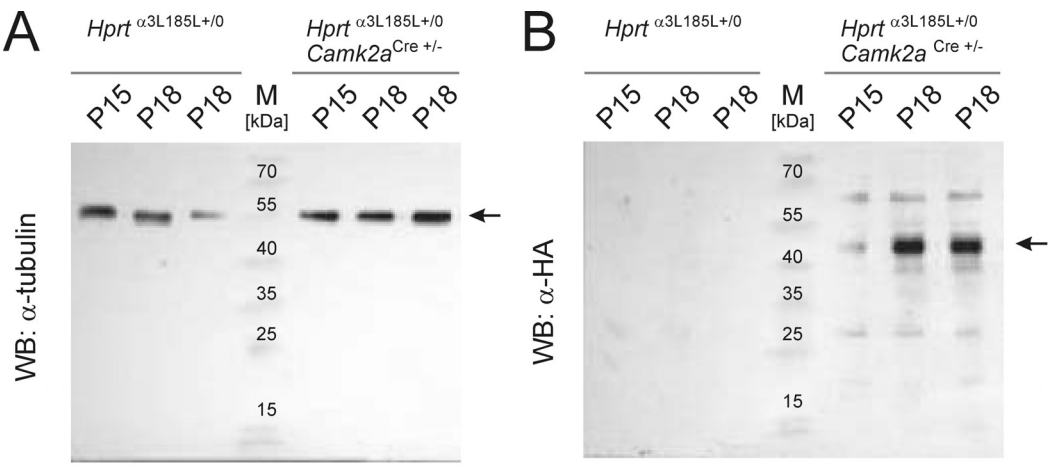

Suppl. Figure 10: GlyR α3L^{185L} protein expression in *Hprt*$^{α3L185L\ +/0}$; *Camk2a*$^{Cre\ +/-}$animals starts around postnatal day (P) 15-18. Slices used for whole cell patch clamp recording of paired-pulse ratios were subject to western blot analysis of tubulin (A) and GlyR HA-α3L^{185L} protein expression (B, α-HA). The band corresponding to full-length (48 kDa) GlyR HA-α3L^{185L} protein is indicated with an arrow.

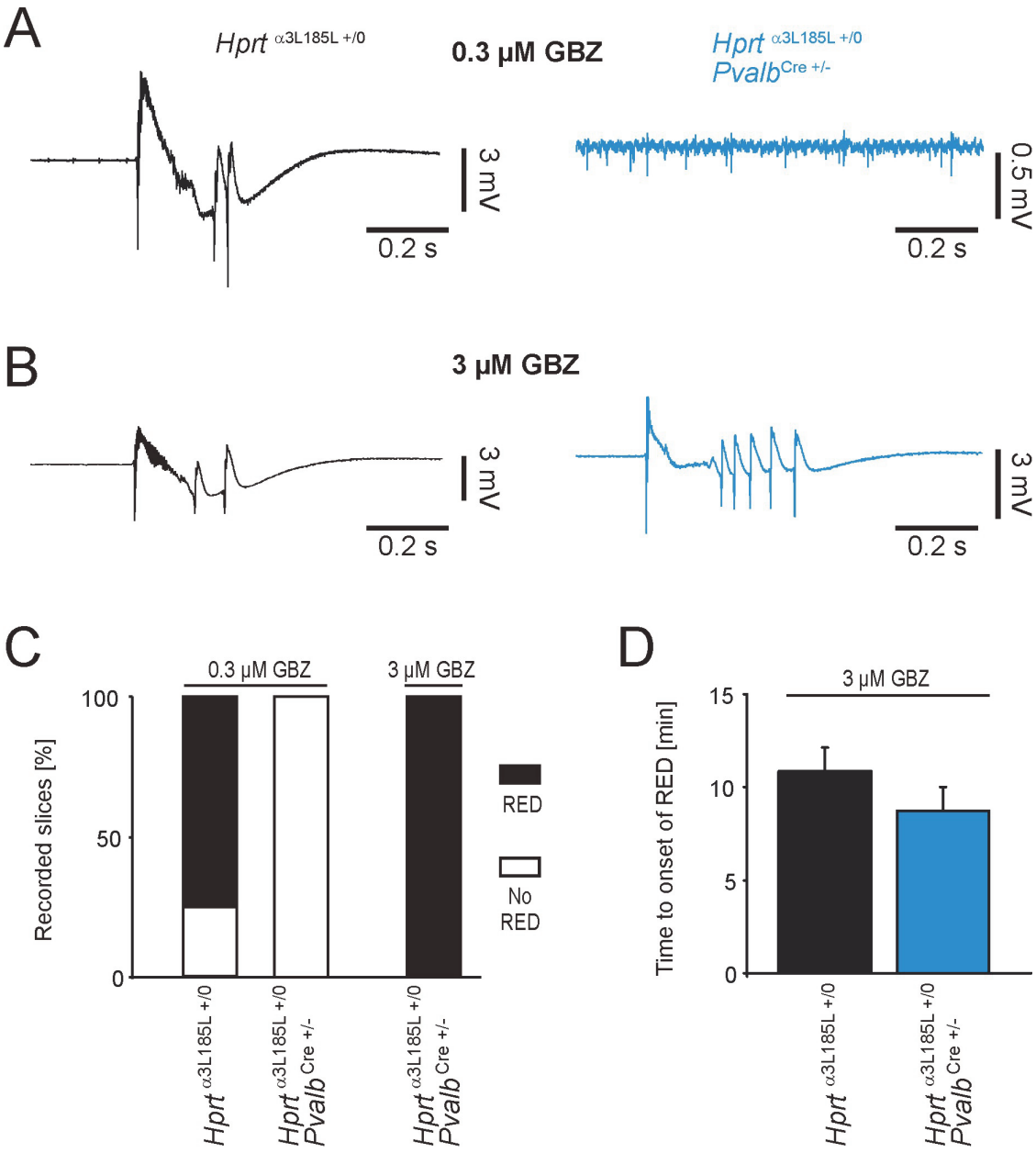

Suppl. Figure 11: Hippocampal network excitability in mice with *Pvalb*^{Cre}-dependent GlyR α3L^{185L} expression. (A, B) Comparison of the effects of different gabazine ('GBZ') concentrations (A, 0.3 µM; B, 3 µM) on incidence of recurrent epileptiform discharge ('RED'). (C, D) Quantification of the percentage of slices with RED (C), and latency to RED (D). Note that a high dose (3 µM) of the competitive $GABA_AR$ antagonist gabazine was required to elicit RED in *Hprt*$^{α3L185L\ +/0}$; *Pvalb*$^{Cre\ +/-}$ mice, while the latency to epileptiform network activity was comparable in control (*Hprt*$^{α3L185L\ +/0}$) and *Hprt*$^{α3L185L\ +/0}$; *Pvalb*$^{Cre\ +/-}$ mice. Data represent means ± standard error.

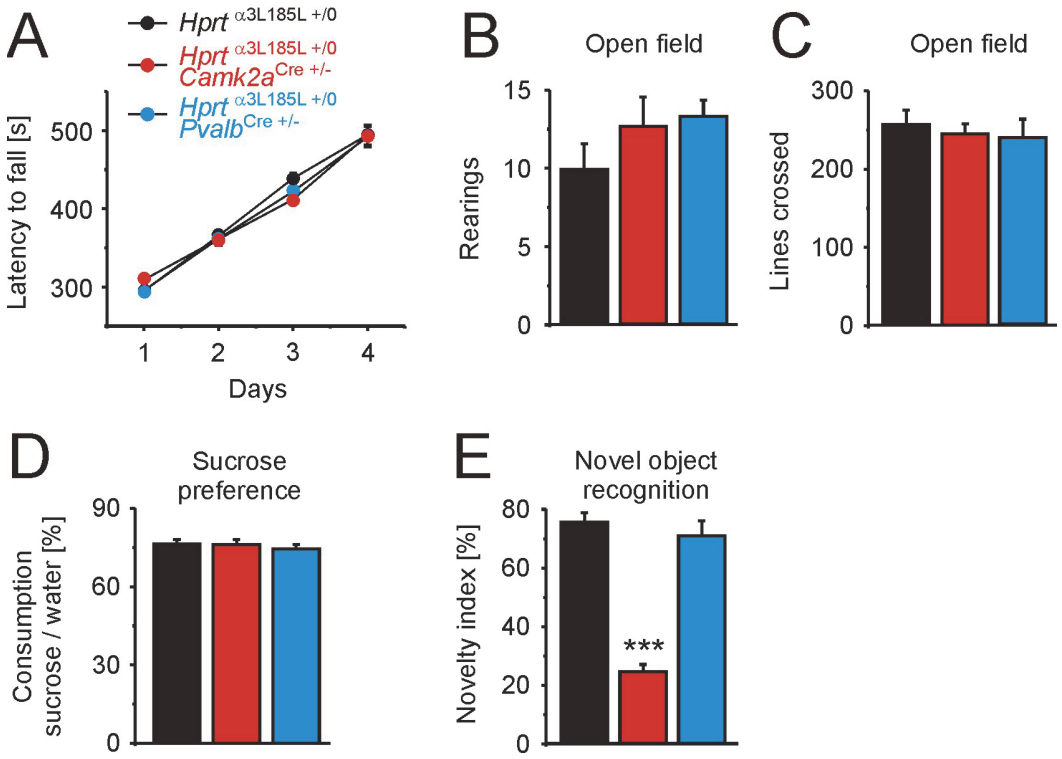

Suppl. Figure 12: Behavioral analysis of motor coordination, sucrose preference and performance in novel object recognition task. (A) Cell type-specific GlyR $\alpha3L^{185L}$ protein expression did not influence motor balance and coordination as the latency to fall was comparable in all cases. Furthermore, training of mice increased their performance (prolonged latency to fall time), which indicates that targeted GlyR $\alpha3L^{185L}$ protein expression did not influence motor learning (procedural memory). (B, C) Locomotor behavior during the open field test did not reveal differences between genotypes (B, rearings; C, lines crossed). (D) All mice preferred sucrose-containing water. (E) Selective impairment of *Hprt*$^{\alpha3L185L\ +/0}$; *Camk2a*$^{Cre\ +/-}$ mice in the novel object recognition test which addresses the ability of mice to discriminate familiar and novel objects (declarative memory). Statistical significance is indicated as ***: $P < 0.001$. Data represent means ± standard error.

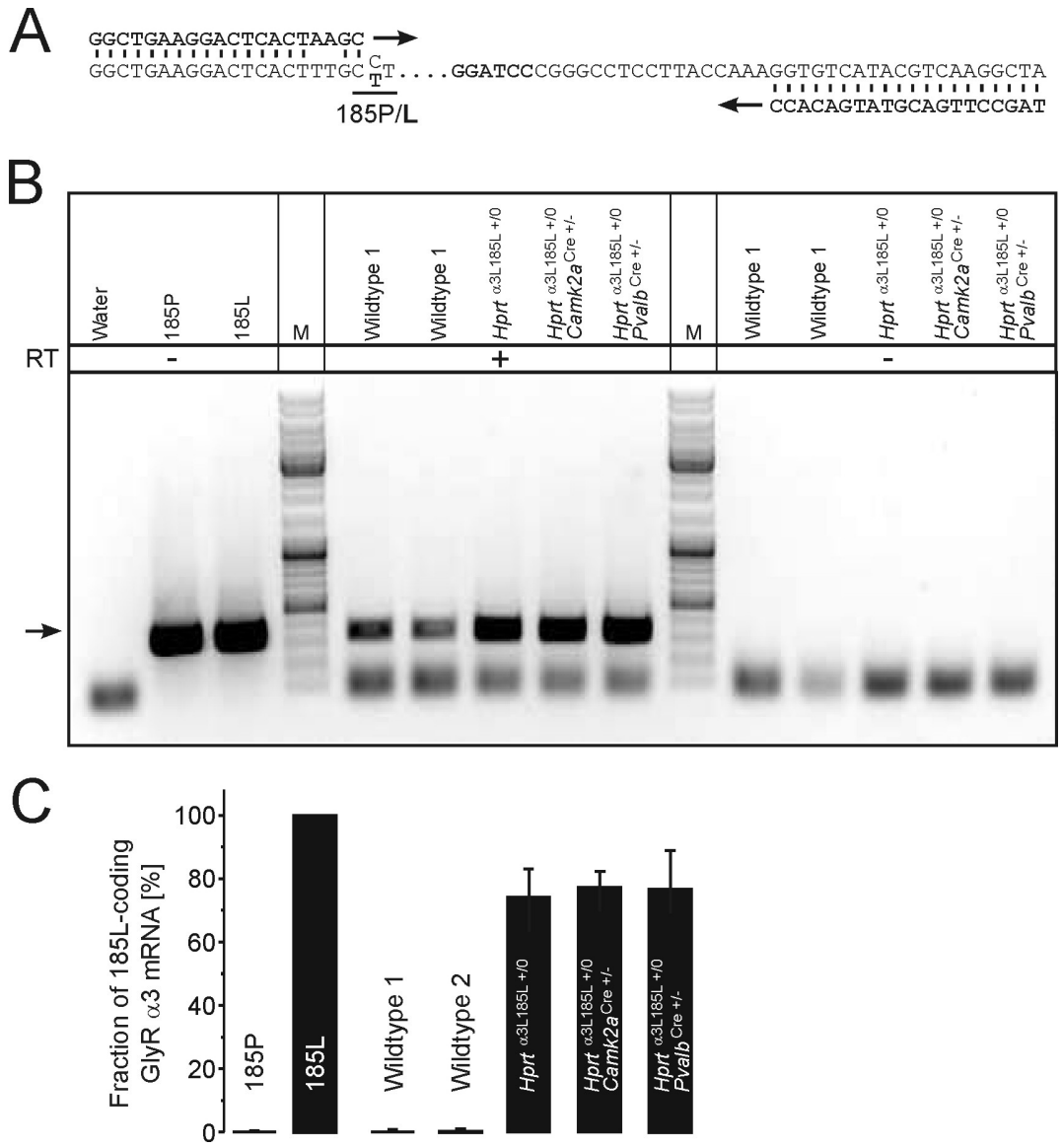

Suppl. Figure 13: Quantification of the fraction of GlyR $\alpha 3^{185L}$-coding mRNAs. (A) Sequence details around the 185L-coding region of GlyR α3 mRNA are shown. The forward PCR oligonucleotide contains a partial *Hind*III restriction enzyme site (AAGC) which is completed to a full site (AAGCTT) if a $\alpha 3^{185L}$-coding cDNA is amplified. The *Hind*III site is used together with GlyR α3-intrinsic *BamH*I site for cloning purpose and quantification relative to the positive (100%) control clone '185L' which was amplified and cloned in parallel with the negative control clone '185P' and mRNA probes. (B) Agarose gel showing amplification products obtained from control clones and mRNA isolated out of hippocampi from wildtype and $Hprt^{\alpha 3L185L\ +/0}$, $Hprt^{\alpha 3L185L\ +/0}$; $Camk2a^{Cre\ +/-}$ and $Hprt^{\alpha 3L185L\ +/0}$; $Pvalb^{Cre\ +/-}$mice. To verify absence of genomic DNA, the reverse transcriptase ('RT -') was omitted. (C) Quantification of the fractions of GlyR $\alpha 3^{185L}$-coding mRNAs. Data represent means ± standard deviation.

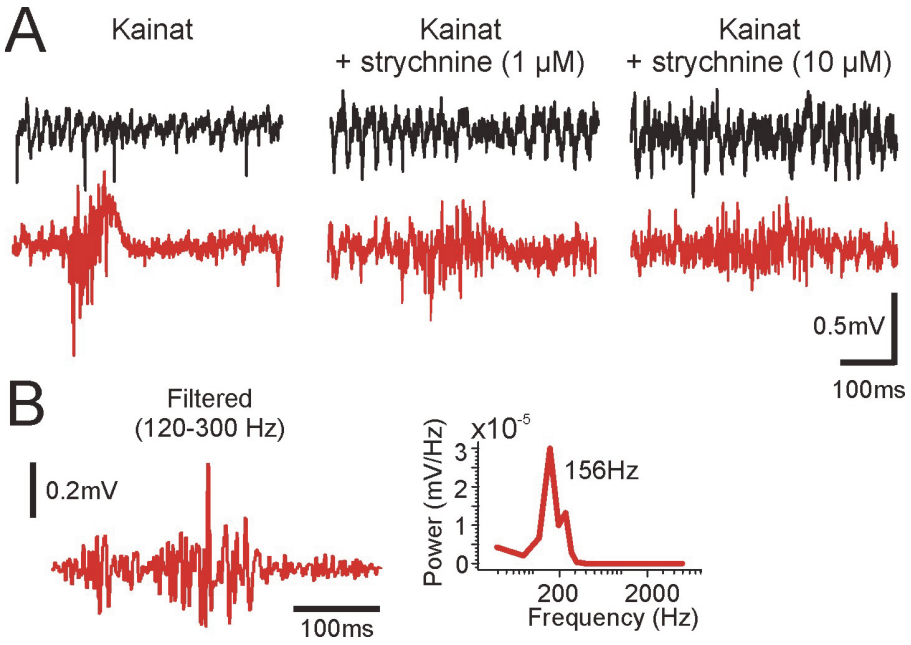

Suppl. Figure 14: High frequency ripple oscillatory activity precedes recurrent epileptiform discharge in *Hprt*$^{\alpha 3L185L\ +/0}$; *Camk2a*$^{Cre\ +/-}$ animals. Black and red colors represent traces obtained from *Hprt*$^{\alpha 3L185L\ +/0}$ and *Hprt*$^{\alpha 3L185L\ +/0}$; *Camk2a*$^{Cre\ +/-}$ animals, respectively. (A) Dose-dependent effects of strychnine on recurrent hyper-synchronous network activity in *Hprt*$^{\alpha 3L185L\ +/0}$; *Camk2a*$^{Cre\ +/-}$ slices. (B) Band-pass filtered trace and power spectrum of the pathological event shown in (A) illustrate characteristics of the high frequency ripple oscillatory component. Note that the hyper-synchronous component was blocked with strychnine (A), while high frequency ripple oscillatory activity (B) preceding the pathological event persisted in the presence of strychnine.

Supplementary References

1. Legendre P, Förstera B, Jüttner R, Meier JC. Glycine receptors caught between genome and proteome - Functional implications of RNA editing and splicing. *Front Mol Neurosci*. 2009;2:23.

2. Melzer N, Villmann C, Becker K, Harvey K, Harvey RJ, Vogel N, Kluck CJ, Kneussel M, Becker CM. Multifunctional basic motif in the glycine receptor intracellular domain induces subunit-specific sorting. *J Biol Chem*. 2010;285:3730-3739.

3. Tang W, Ehrlich I, Wolff SB, Michalski AM, Wolfl S, Hasan MT, Luthi A, Sprengel R. Faithful expression of multiple proteins via 2A-peptide self-processing: a versatile and reliable method for manipulating brain circuits. *J Neurosci*. 2009;29:8621-8629.

4. Meier JC, Henneberger C, Melnick I, Racca C, Harvey RJ, Heinemann U, Schmieden V, Grantyn R. RNA editing produces glycine receptor α3P185L resulting in high agonist potency. *Nat Neurosci*. 2005;8:736-744.

5. Eichler SA, Kirischuk S, Jüttner R, Schäfermeier PK, Legendre P, Lehmann TN, Gloveli T, Grantyn R, Meier JC. Glycinergic Tonic Inhibition of Hippocampal Neurons with Depolarising GABAergic Transmission Elicits Histopathological Signs of Temporal Lobe Epilepsy. *J Cell Mol Med*. 2008;12:2848-2866.

6. Giovannoni R, Maggio N, Rosaria BM, Cavaliere C, Cirillo G, Lavitrano M, Papa M. Reactive astrocytosis and glial glutamate transporter clustering are early changes in a spinocerebellar ataxia type 1 transgenic mouse model. *Neuron Glia Biol*. 2007;3:335-351.

7. Strekalova T, Spanagel R, Bartsch D, Henn FA, Gass P. Stress-induced anhedonia in mice is associated with deficits in forced swimming and exploration. *Neuropsychopharmacology*. 2004;29:2007-2017.

8. Walf AA, Frye CA. The use of the elevated plus maze as an assay of anxiety-related behavior in rodents. *Nat Protoc*. 2007;2:322-328.

9. Anagnostaras SG, Murphy GG, Hamilton SE, Mitchell SL, Rahnama NP, Nathanson NM, Silva AJ. Selective cognitive dysfunction in acetylcholine M1 muscarinic receptor mutant mice. *Nat Neurosci*. 2003;6:51-58.

10. Dix SL, Aggleton JP. Extending the spontaneous preference test of recognition: evidence of object-location and object-context recognition. *Behav Brain Res*. 1999;99:191-200.

11. Zlomuzica A, Ruocco LA, Sadile AG, Huston JP, Dere E. Histamine H1 receptor knockout mice exhibit impaired spatial memory in the eight-arm radial maze. *Br J Pharmacol*. 2009;157:86-91.

Co-sedimentation /

Full unedited gels for Figure 1